NANO LETTERS

2008
Vol. 8, No. 1
49−55

Role of Molecular Surface Passivation in Electrical Transport Properties of InAs Nanowires

Qingling Hang,[†] Fudong Wang,[‡] Patrick D. Carpenter,[†] Dmitri Zemlyanov,[†] Dmitri Zakharov,[†] Eric A. Stach,[†] William E. Buhro,[‡] and David B. Janes*,[†]

Birck Nanotechnology Center, Purdue University, West Lafayette, Indiana 47907, and Department of Chemistry and Center for Materials Innovation, Washington University, St. Louis, Missouri 63130

Received August 2, 2007; Revised Manuscript Received November 1, 2007

ABSTRACT

The existence of large densities of surface states on InAs pins the surface Fermi level above the conduction band and also degrades the electron mobility in thin films and nanowires. Field effect transistors have been fabricated and characterized in the "as fabricated" state and after surface passivation with 1-octadecanethiol (ODT). Electrical characterization of the transistors shows that the subthreshold slope and electron mobility in devices passivated with ODT are superior to the respective values in unpassivated devices. An X-ray photoelectron spectroscopy study of ODT passivated undoped InAs nanowires indicates that sulfur from ODT is bonded to In on the InAs nanowires. Simulations using a two-dimensional device simulator (MEDICI) show that the improvements in device performance after ODT passivation can be quantified in terms of a decrease of interface trap electron donor states, shifts in fixed interfacial charge, and changes in body and surface mobilities.

InAs is a very interesting semiconducting material, which has potential applications in high-speed circuits and other special devices, like superconductor/normal conductor/superconductor Josephson junction devices[1−4] and dilute magnetic semiconductor devices.[5−7] However, in InAs, as in other III−V semiconductors, there are a large number of surface states, which pin the InAs surface Fermi level in the conduction band, resulting in a surface accumulation layer of electrons. Various organic and inorganic approaches for passivating thin film or bulk InAs have been reported.[8−11] Passivation with inorganic sulfide or thioacetamide does not eliminate the surface accumulation layer significantly.[10] Raman spectroscopy studies indicate that the adsorption of alkanethiols molecules on InAs unpins the Fermi level,[11] which implies a significant reduction of surface states.

It is not surprising that p channel conduction has been difficult to achieve in InAs nanowire field effect transistors (NWFETs) due to the Fermi level pinning above the conduction band.[12] We have recently demonstrated ambipolar (p and n channel) conduction in NWFETs employing 20 nm Cd doped InAs nanowires encapsulated during growth with surface ligands and shown n channel conduction after removal of the ligands by oxygen plasma.[13]

In thin film InAs devices, the surface accumulation layer has a relatively low mobility, resulting in an overall channel mobility that decreases with decreasing layer thickness.[14] Though reports of mobilities in InAs nanowires are somewhat limited, it appears that the mobility decreases with decreasing nanowire diameters with values of about 3000 $cm^2/(V\ s)$ reported for 80 nm diameter,[15] 1500 $cm^2/(V\ s)$ for 50 nm diameter,[16] and about 200 $cm^2/(V\ s)$ for 25 nm diameter.[17] This trend is expected to become worse when the diameter of nanowires is less than one electron de Broglie wavelength, which is 40 nm for bulk InAs.[18] For a 20 nm diameter nanowire, this means that all of the body electrons will be scattered by interactions with the surface, blurring the distinction between body electrons and surface electrons. InAs nanowires with diameters larger than one de Broglie wavelength should contain a central region with the macroscopic properties of InAs. This accounts, in part, for the observation of lower mobilities in InAs nanowires with diameters of 50 nm and below.

In this study, we have fabricated FETs from individual 20 nm, undoped InAs nanowires and shown that relatively high mobility can be realized in nanowires passivated with 1-octadecanethiol (ODT). X-ray photoelectron spectroscopy (XPS) studies of the ODT passivated nanowires indicate that ODT molecules are bound to InAs nanowires through In−S bonds. The formation of these In−S bonds is believed

* Corresponding author. E-mail: janes@ecn.purdue.edu.
[†] Purdue University.
[‡] Washington University.

10.1021/nl071888t CCC: $40.75
Published on Web 12/04/2007

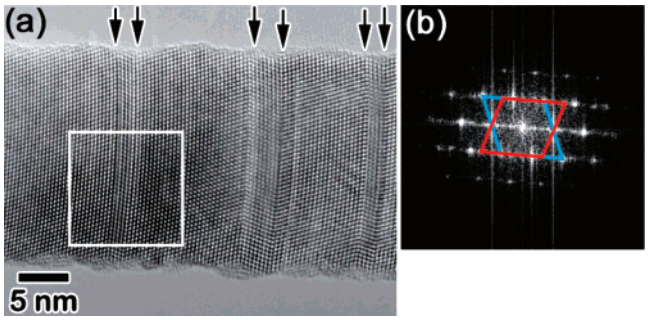

Figure 1. (a) High-resolution transmission electron microscope image of as-synthesized 20 nm undoped InAs nanowire. The arrows indicate the location of twin defects. (b) Diffractogram taken from the white box in (a). The blue and red parallelograms are used to demonstrate that the lattice defect is a twin.

to passivate the surface states on the nanowires, so that the body electrons experience less scattering due to surface states.

InAs nanowires were synthesized from 44 nm diameter Bi nanoparticles (containing 0.003 mmol Bi atoms) in polydecene (4.5 g) by the solution−liquid−solid (SLS) method, using conditions comparable to previous reports.[13,19] $In(myristate)_3$ (0.282 mmol) and $As(SiMe_3)_3$ (0.161 mmol) were used as the In and As precursors, respectively, and 1-hexadecylamine (HDA, 1.26 mmol) and tri-*n*-octylphospine (TOP, 0.243 mmol) were used as additional surfactants. The nanowires were synthesized at 304 °C and were nominally undoped. These nanowires were passivated with HDA molecules, which could be easily removed from the nanowires by ultrasonication. The nanowires exhibited the zinc blende crystal structure and the d-spacings determined from powder X-ray diffraction were $d_{111} = 3.5147$ Å, $d_{220} = 2.1455$ Å, and $d_{311} = 1.8295$ Å. The theoretical *d* spacings of bulk InAs materials are $d_{111} = 3.4980$ Å, $d_{220} = 2.1420$ Å, and $d_{311} = 1.8263$ Å.[20] The difference between the measured and theoretical values is within the range of experimental uncertainty. Figure 1a shows a high-resolution transmission electron microscope image (HRTEM) of a representative as-synthesized 20 nm undoped InAs nanowire. Multiple twin defects along the nanowire are indicated by arrows in the image. Similar twin defects have been reported in GaP nanowires synthesized by metal−organic vapor-phase epitaxy.[21,22] The surface of the nanowire exhibits corrugations along local ⟨111⟩ directions as well as <1 nm of a disordered/amorphous phase. As discussed later, this surface layer appears to consist of In and As oxides.

The InAs NWFETs were fabricated using previously reported procedures,[13] using a 40 nm SiO_2 gate insulator over a heavily doped p-type Si substrate, and Ni source/drain contacts. Prior to deposition in devices or XPS characterization, the nanowires were purified by ultrasonication (1 min) in a mixture of toluene and 2-propanol, followed by centrifugation, with the ultrasonication−centrifugation process repeated three times. The isolated nanowires were then dispersed in the mixture of toluene and 2-propanol for subsequent device fabrication. Following fabrication, the InAs nanowires within the FET structures were passivated with ODT using the following procedure. The device wafer was dipped in a 1:1 (v/v) solution of deionized (DI) water and 49 wt % HF for 2 s, rinsed in DI water, dipped in ethanol, and then immediately put in a 5 mM ODT solution in ethanol.[23] After 24 h in the solution, the wafer was removed and rinsed with ethanol.

The ODT-passivated wires for XPS characterization were prepared separately as follows. The purified wires (about 1 mg) as described above were washed with ethanol four times. An ODT−ethanol solution (5 mM, 7 mL) was added to the suspension of the purified wires in ethanol (2 mL), followed by an HF−ethanol solution (1.2 M, 1 mL) with stirring. After over 24 h this nanowire solution was purified with ethanol by centrifugation for five times, followed by deposition of the nanowires on a gold surface. Note that somewhat different procedures were used in the preparation of XPS samples because the solution-based techniques did not allow as short of an HF exposure as was used in treatments on the fabricated devices.

The XPS data were obtained using a Kratos Ultra DLD spectrometer using monochromatic Al Kα radiation ($h\nu = 1486.58$ eV) and fixed analyzer pass energy of 160 eV for survey spectra and 20 eV for high-resolution spectra. The XPS spectra were analyzed by CasaXPS software version 2.3.12. The spectra were curve-fitted assuming Gaussian−Lorentzian line shape. The atomic concentrations of the chemical elements in the near-surface region were estimated after the subtraction of a Shirley type background, taking into account the corresponding Scofield atomic sensitivity factors and empirically chosen attenuation function to compensate the different attenuation length for the photoelectrons emitted from the different electron levels. The binding energy (BE) values referred to the Fermi level were calibrated using Cu 2p and Au 4f lines. Typical resolution measured as a full width at half-maximum (fwhm) of the Au 4f peaks was 0.65 eV. To avoid differential charging, the sample was disconnected from the ground and XPS spectra were acquired using the Kratos charge neutralizer. The charge was then compensated by setting the Au $4f_{7/2}$ peak at 84.0 eV or by setting the C 1s peak at 285.0 eV, if the Au 4f peaks were not detectable.

Room-temperature electrical measurements were performed on an HP 4156A semiconductor parameter analyzer. Figure 2 shows the measured transfer characteristics at a drain/source voltage $V_{DS} = 0.1$ V for a representative InAs NWFET with channel length 3 μm. Curves are shown for the device in the as-fabricated state and after passivation with ODT. The as-fabricated device shows n channel conduction, with an inverse subthreshold slope (SS) of 3.5 V/decade and a field-effect mobility (μ_{FE}) of 740 $cm^2/(V\ s)$, inferred from extraction using the measured transconductance and a cylinder-over-plate capacitance model.[13,24] The low mobility of our InAs nanowire devices compared to bulk InAs may be partly from the twin defects observed in the HRTEM image. To passivate the large number of surface states and reduce the scattering of the body electrons with surface states, the same device was passivated with ODT as described above. The transfer characteristic showed an improvement

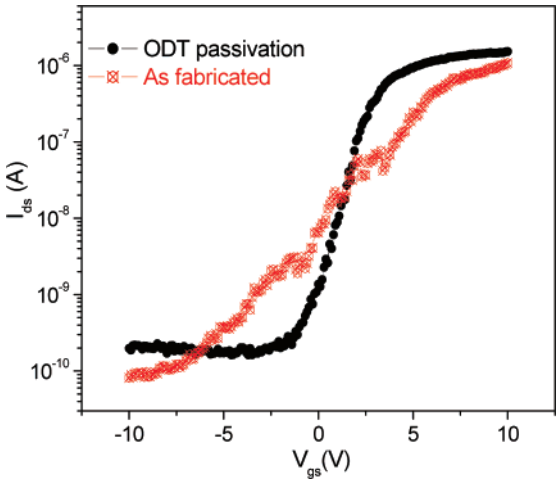

Figure 2. Transfer characteristics at $V_{ds} = 100$ mV of field effect transistor containing a single, 20 nm diameter InAs nanowire before and after ODT molecular passivation.

Table 1: Atomic Concentration of Elements Determined by XPS from Area 1 with ODT Passivated InAs Nanowires and Area 2 without Nanowires

	S 2p	O 1s	In 3d	As 3d	C 1s	Au 4f
area 1	1.8	6.1	5.6	3.4	80.1	3.0
area 2	1.0	8.5	0.0	0.0	65.5	25.5

in SS (1.0 V/decade), and the μ_{FE} increased to 1235 cm^2/(V s) for the device after passivation.

The improvement of μ_{FE} and SS is believed to be associated with a reduction of InAs surface states due to the bonding of the ODT molecules. Nanowires with and without ODT passivation have been characterized by XPS. XPS studies on the purified wires showed no measurable nitrogen signature, which would be observed if HDA were present, indicating that the wires were no longer passivated by ligands. For XPS measurements, nanowires passivated with ODT have been deposited from suspension on a gold substrate. Because the entire Au surface was exposed to the solution containing ODT, control XPS spectra were acquired from the part of the Au surface that visually did not have nanowires. By repeatedly dropping nanowire solution onto a specific area, a dense multilayer mat of nanowires was formed on the gold surface (denoted area 1). In other regions on the surface (area 2), a much smaller number of nanowires, which is mainly from the diffusion of ethyl alcohol on the Au surface, was observed. Table 1 shows the atomic concentration of elements in these two areas inferred from XPS measurements. In and As were found in area 1, but not in area 2, as expected. Within the XPS detection sensitivity, we can conclude that area 2 is free of InAs nanowires. The significantly lower Au concentration, 3.0% in area 1 versus 25.0% in area 2, indicates that there are thick layers of InAs nanowires in area 1. In addition, the larger amounts of C and S within area 1 are consistent with ODT bound to the nanowires, although the observation of both C and S within area 2 indicates that ODT molecules have also bonded to the Au surface. Likely some amount of ODT remained in the nanowire/ethyl alcohol solution, even though the ODT

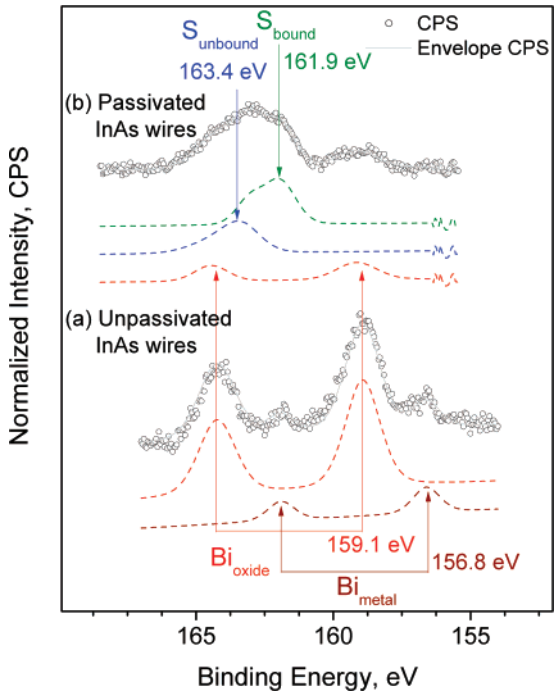

Figure 3. XPS spectra showing S 2p and Bi 4f peaks for (a) unpassivated nanowires and (b) nanowires with ODT passivation.

solution was nominally replaced by ethyl alcohol. The decrease of oxygen content in area 1 could be explained by passivating effects of ODT, which prevents oxidation of the InAs nanowire. On the basis of the relative amplitude of the Au signals in the two areas, the contribution to the C and S peaks from regions within area 1 that are not covered with nanowires is estimated to be 10−12%. On this basis, we can conclude that the data from area 1 are primarily associated with the nanowires. In the case of the unpassivated InAs nanowires, the layer was homogeneous enough to screen the substrate completely.

Figures 3−5 show the S 2p/Bi 4f, As 3d, and In 3d core level spectra obtained from unpassivated and ODT passivated InAs nanowires, with the passivated data obtained from area 1. As represented in Figure 3, the unpassivated nanowires demonstrate the presence of Bi, which originates from Bi particles at the nanowire tips. Two chemical states of bismuth are distinguishable: the Bi $4f_{7/2}$ peak at 156.8 eV corresponding to a metallic state and the Bi $4f_{7/2}$ peak at 159.1 eV corresponding to an oxidized state. The separation in the Bi 4f doublet was assumed to be 5.30 eV. The ODT passivated nanowires also show the presence of sulfur, which also exists in two chemical states. Assuming the S 2p doublet separation to be 1.10 eV, the S $2p_{3/2}$ peak at 161.9 eV corresponds to sulfur covalently bound to InAs nanowires, and the S $2p_{3/2}$ peak at 163.4 eV originates from sulfur that is not bound to the surface. Peaks associated sulfur oxides would be expected at binding energies above 166 eV;[25] the lack of a peak in this range in Figure 3b indicates that there is not significantly bonding between S and O. Similar thiol adsorption has been reported on Au surfaces.[25]

The As 3d spectra for unpassivated and ODT-passivated nanowires are shown in Figure 4. For the unpassivated

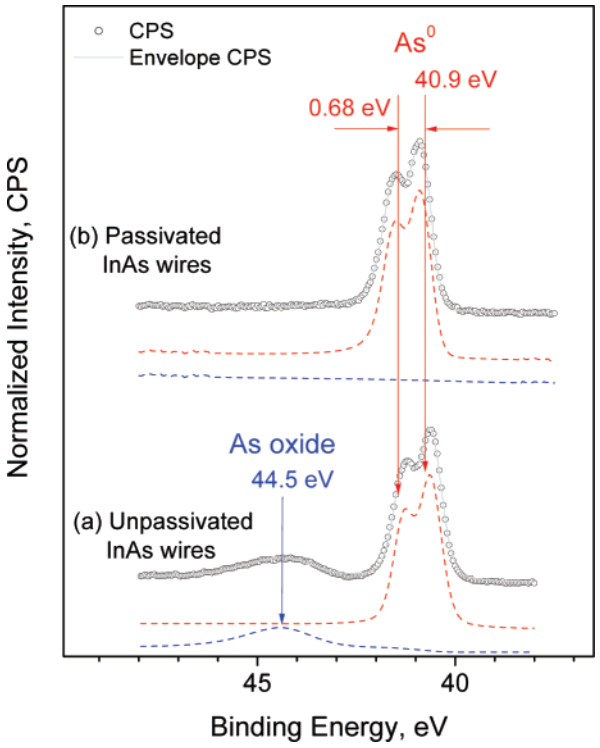

Figure 4. XPS spectra showing As 3d peaks for (a) unpassivated nanowires and (b) nanowires with ODT passivation. An As oxide peak is observed at 44.5 eV in the unpassivated nanowires, but not in the passivated nanowires.

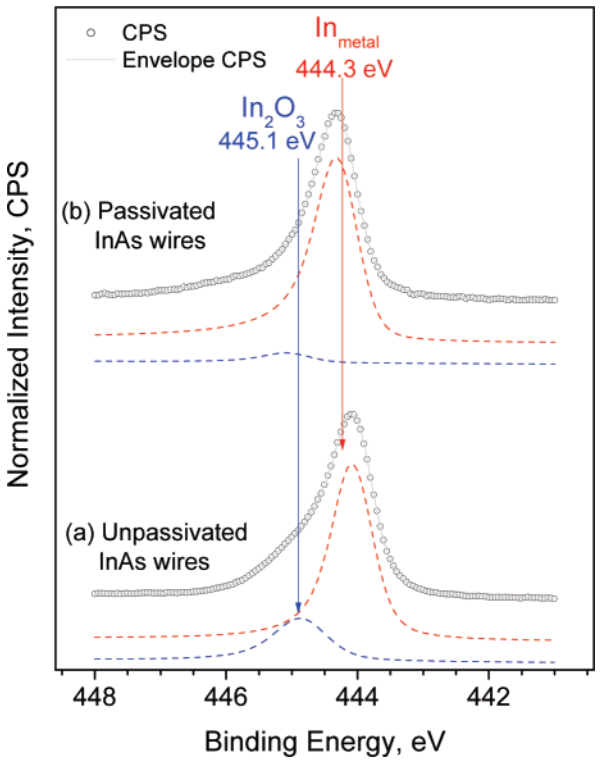

Figure 5. XPS spectra showing In 3d5/2 peaks for (a) unpassivated nanowires and (b) nanowires with ODT passivation.

nanowires, XPS detects AsO_x and As characterized by the As $3d_{5/2}$ peaks at 44.5 and 40.9 eV with doublet separation 0.68 eV, respectively. The As 3d peaks of non-oxidized arsenic are in good agreement with a prior XPS study on a (100) InAs wafer,[26] and the peaks were assigned to As bound to In. The ratio between the areas of the As 3d peaks for the nonoxidized state and AsO_x is approximately 4, whereas the same ratio calculated from the As $2p_{3/2}$ components (spectra not shown here) is equal to 0.6. The different inelastic mean free path (IMFP) for photoelectrons emitted from the 3d and 2p core levels is 29.84 Å[27] and 6.68 Å, respectively, indicating that the AsO_x is at the surface. The increased contribution of the AsO_x components with decreasing IMFP can be therefore assigned to the surface nature of the oxide phase. No oxide phase was found on the ODT passivated nanowires (Figure 4b). The absence of the peak at ~43 eV corresponding to a As−S bond[28−30] indicates that S does not bind to As.

Figure 5 shows the In $3d_{5/2}$ spectra obtained from InAs nanowires with and without ODT passivation. For the unpassivated nanowires, the In $3d_{5/2}$ spectrum can be curve-fit by two components at 444.3 and 445.1 eV, corresponding to an In−As bond and In_2O_3 binding states, respectively. The In $3d_{5/2}$ spectrum obtained from ODT passivated InAs nanowires does not exhibit a pronounced high binding energy shoulder as observed in unpassivated nanowires but shows a weak component at ~445.0 eV. Due to the relatively low intensity of this peak and the small binding energy difference between the In_2O_3 and InS_x binding states (this is also true for thioacetamide passivated InAs wafer),[26] it is difficult to state definitely that ODT binds to the nanowire by considering exclusively the In 3d spectra. However, on the basis of the lack of peaks corresponding to As−S and S−O, it appears that sulfur binds to In, that is to say, ODT molecules bind to InAs nanowires primarily through In−S bonds. This is consistent with the prior report of thioacetamide passivation of planar (100) InAs surface.[26]

For InAs nanowires without molecular passivation, the XPS results indicate In_2O_3 and AsO_x on the surface, which agrees with the characterization of bulk InAs.[28] For nanowires with ODT passivation, no significant oxidation is observed; presumably the ODT−In surface layer prevents the oxidation of In and As. It therefore inferred for InAs nanowires that AsO_x and/or In_2O_3 are responsible for the surface Fermi level pinning. For ODT passivated nanowires there are less surface states, which lead to reduced surface state scattering.

The improvement of SS and μ_{FE} after ODT passivation of InAs nanowires can be attributed to the change of surface states on the InAs nanowire surface. Although absorbed molecular layers on Au can modify the effective work function of the exposed Au surface, the local work function at the metal to nanowire interface is not expected to change significantly. Generally speaking, there are two kinds of charges, fixed charges and interface trap charges at the surface of nanowires, which affect the transfer characteristics of the FETs, modifying the threshold voltage and the SS. It is well-known that fixed charges near the gate side are responsible for the shift of the threshold voltage, and interface trap charges can change the SS. It has been pointed out in SiC thin film FETs that the degradation of field effect mobility is due to interface trap electron acceptor charges at the interface between gate dielectric and SiC thin film.[31]

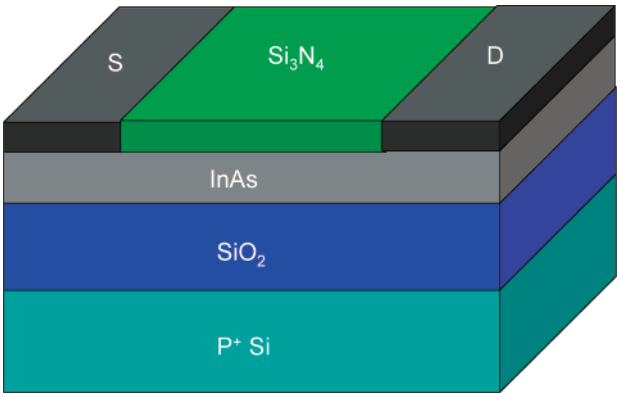

Figure 6. Device structure for MEDICI simulation. The InAs slab is 20 nm thick and 55 nm wide. The SiO_2 dielectric is 40 nm thick. Q_{it1} refers to the interface trap charge states at the interface between oxide and InAs. Q_{it2} refers to the interface trap charges at the exposed nanowire surface. Q_{f1} and Q_{f2} refer to the fixed charges at the oxide/InAs interface and the exposed surface.

We used the MEDICI semiconductor device simulation software[32] to quantitatively relate the changes in device performance following ODT passivation to surface states and charges on the nanowire surfaces/interfaces. The device structure used to simulate our InAs nanowire FET is shown in Figure 6. We used InAs material parameters from ref 18, for instance, static permittivity 15.15, electron affinity 4.9 eV, energy band gap 0.354 eV, conduction band effective density of states $8.7 \times 10^{16}/\text{cm}^3$ and valence band effective density of states $6.6 \times 10^{18}/\text{cm}^3$. The doping concentration was assumed to be $2 \times 10^{16}/\text{cm}^3$ according to ref 14 for unintentionally doped InAs thin film. The channel length was set to 3 μm, the same as the actual device. The MEDICI simulation is a 2-D simulation (effectively a vertical plane running from source to drain) and effectively assumes that the structure is uniform in a direction perpendicular to this plane. Although the effects of charge on the side walls are not considered, the overall nanowire geometry can be approximated by utilizing an effective width (W_{EFF}) determined by equating the capacitance predicted by MEDICI (capacitance per unit width times W_{EFF}) with that calculated from the cylinder-over-plate model for the cylindrical geometry.[13,24] For the nanowire diameter and oxide thickness in the current devices, a capacitance of 2.85×10^{-16} F is calculated from the cylinder-over-plate model, corresponding to a W_{EFF} of 55 nm in the MEDICI simulation. Note that W_{EFF} is larger than the nanowire diameter due to fringing effects, which are not considered in the 2-D MEDICI simulation. In addition, as long as the device is turned on ($V > V_T$ (threshold voltage)), the capacitances inferred from MEDICI simulations for device structures with or without surface charges are the same. This is confirmed by calculating the number of carriers per unit area in the channel versus gate voltage for voltages larger than V_T. To incoporate surface charges on the top surface, the simulation includes a layer of silicon nitride on top of the channel, which is electrically floating. From the calculated band diagrams, there is no obvious band bending in the nitride. In the simulation, only electrons are considered as current carriers and the comparisons to the experimental data were performed only in the regions exhibiting clear n-channel behavior. In the simulation, separate mobility values are set for the body and surface electrons. Here the contact resistance is not expected to play an important role in the on-state characteristics of the NWFETs, because the contacts between Ni and InAs (without molecular passivation for the contact segments) should have small resistance.[12] The surface Fermi level pinning implies that there are interface trap states on the InAs surface which behave as electron donors. In our simulation, we use such trap states at the top and bottom nanowire surfaces and assume that these trap states are distributed uniformly in energy throughout the band gap. For the nanowire geometry, which is comparable to a floating-body silicon-on-insulator (SOI) structure, both the voltage-variable interface trap charges and the fixed charges at the interface opposite to the gate side contribute to changes in the SS, which is reasonable considering that the number of interface trap charges varies with gate bias and the fixed charges on the opposite side of gate side contribute to the capacitance of the InAs slab. However, the fixed charges at the gate side shift the V_T but do not contribute to the changes in subthreshold slope.

Figures 7 and 8 show the measured transfer curves for as-fabricated and ODT-passivated InAs NWFETs, along with the best-fit MEDICI simulation result, on a log scale of I_{ds} (Figures 7a, 8a) to show the fitting of subthreshold slope and on a linear scale (Figures 7b, 8b) for I_{ds} to show the fitting of the on-state of the device. In each case, the parameters used in the corresponding MEDICI simulation are shown in the inset. For the unpassivated devices, the interface trap densities are $1.5 \times 10^{13}/(\text{cm}^2\ \text{eV})$ (Q_{it1}) and $1.0 \times 10^{13}/(\text{cm}^2\ \text{eV})$ (Q_{it2}) for the bottom and top InAs surfaces, respectively. For the ODT passivated device, the trap densities decrease to $7 \times 10^{12}/(\text{cm}^2\ \text{eV})$ (Q_{it1}) and $5 \times 10^{12}/(\text{cm}^2\ \text{eV})$ (Q_{it2}). The reduction in trap density is believed to be due to the chemical bonding between the S in the ODT and In on the nanowire surface. This decrease is consistent with the claim that the surface Fermi level is not pinned in the conduction band for the passivated nanowires. A significant reduction is also observed in the magnitude of the fixed charge density (Q_f) on the bottom InAs surface for the passivated device (Q_{f1}), whereas the fixed charge density at the exposed side of InAs nanowire (Q_{f2}) increased in magnitude from $-0.2 \times 10^{12}/\text{cm}^2$ to $-0.3 \times 10^{12}/\text{cm}^2$. Because ODT is not expected to add a net charge, the mechanism of this shift in fixed charge is not clear. However, it should be noted that a fixed charge dipole, such as that likely induced upon In−S bonding, will also contribute a shift in threshold that can be modeled as a change in fixed charge density. The body electron mobility (μ_{bulk}) increases from 2100 to 3200 $\text{cm}^2/(\text{V s})$ after passivation, which is reasonable considering the decrease of interface trap charges, which should decrease the scattering of body electrons by these impurity charges, given the de Broglie wavelength of 40 nm discussed earlier. To fit the roll-off in I_{ds} at large V_{gs} values (Figure 8b), a surface electron mobility ($\mu_{surface}$) of 32 $\text{cm}^2/(\text{V s})$ was used for the passivated device. This is

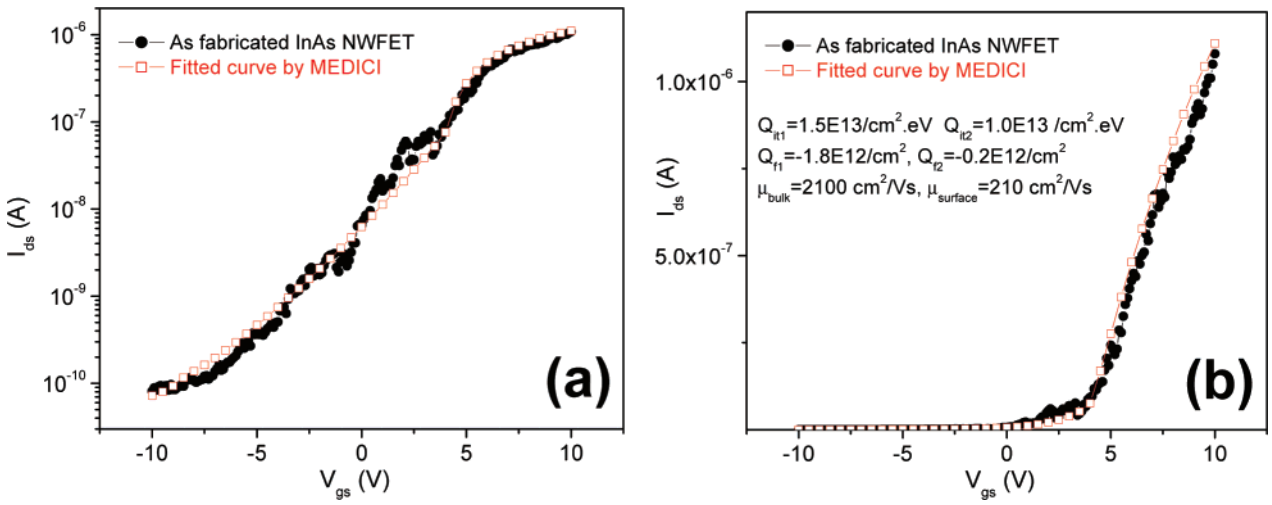

Figure 7. Transfer characteristics for as-fabricated NWFET, showing measured data (closed circles) and best-fit MEDICI simulations (open squares): (a) log scale showing the fitting of subthreshold slope and (b) linear scale showing the fitting of device turn-on. Fitting parameters are shown in the inset.

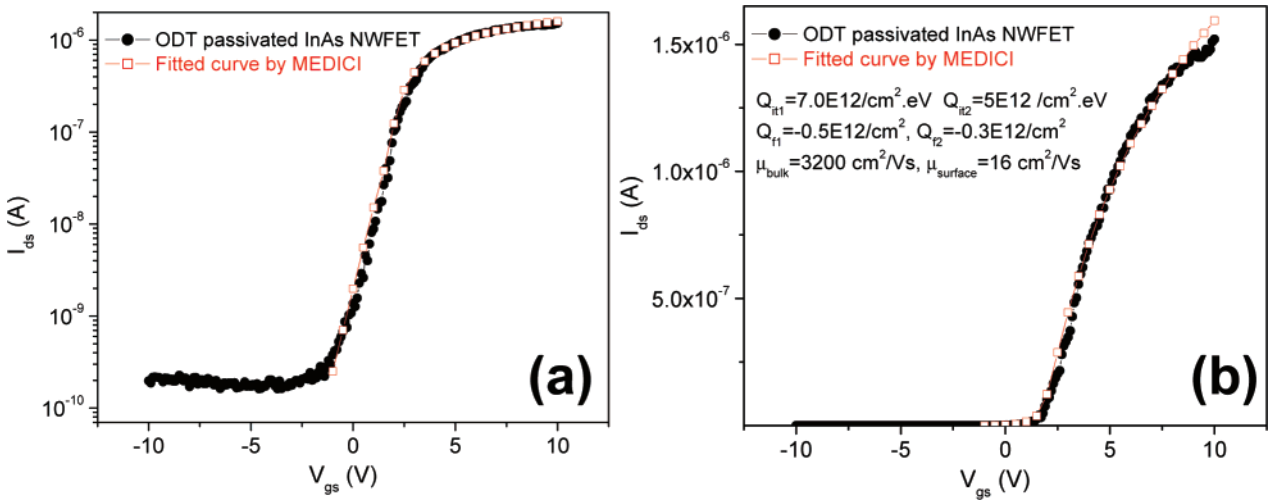

Figure 8. Transfer characteristics for ODT passivated NWFET, showing measured data (closed circles) and best-fit MEDICI simulations (open squares): (a) log scale showing the fitting of subthreshold slope and (b) linear scale showing the fitting of device turn-on. Fitting parameters are shown in the inset.

lower than the value of 210 cm^2/(V s) obtained for the unpassivated device, which may be due to a rougher interface after ODT passivation. Note that the body mobilities obtained from both unpassivated and passivated devices are larger than the mobility determined from the calculation using the cylinder-over-plate capacitance formula. The MEDICI values are believed to be more meaningful, because they consider the effects of both the interface states and the body versus surface mobility. The ratio between surface and body mobility values inferred from the two techniques is smaller for the passivated wires, as expected due to the smaller interface state density in this case.

Although the models proposed for the interface states responsible for Fermi level pinning[33−35] are typically applied to the case of Schottky contacts, the extrinsic models explain the effects in terms of defect states native to the semiconductor. For the case of unmetallized surfaces considered in this paper, the more relevant prior studies involve sidewall passivation in semiconductor devices and semiconductor heterostructures such as GaAs/AlGaAs heterojunctions. In the case of III−V semiconductors, it has been noted that it is possible to achieve unpinned interfaces in epitaxial heterostructures, due to the relatively low densities of interface states that occur at well-matched interfaces.[36] For the case considered in this paper, the S−In bonds at the nanowire surface likely reduce the interface state density due to bonding characteristics comparable to those in an epitaxial heterojunction, although the overall interface density is still somewhat higher than that expected for a well-matched heterointerface.

In conclusion, ODT passivation of InAs nanowires is effective in passivating surface states and increasing the body mobility. The passivated devices exhibited improved subthreshold slopes. XPS characterization indicates that ODT molecules are bound to the InAs nanowire surface through In−S bonds and that the passivated nanowires show negligible surface oxidation. MEDICI simulation allows quantification of the effects of ODT passivation, in terms of

reducing the interface trap charge states and increasing the body electron mobility.

Acknowledgment. We thank Adina Scott and Kangho Lee for help in XPS sample preparation and molecular deposition. This work was supported in part by NASA under URETI grant NCC 2-1363 and by NSF (CHE-0518427).

References

(1) Doh, Y.; van Dam, J. A.; Roest, A. L.; Bakkers, E. P. A. M.; Ouwenhoven, L. P. *Science* **2005**, *309*, 272.
(2) Takayanagi, H.; Kawakami, T. *Phys. Rev. Lett.* **1985**, *54*, 2449.
(3) Kawakami, T.; Takayanagi, H. *Appl. Phys. Lett.* **1985**, *46*, 92.
(4) Kleinsasser, A. W.; Jackson, T. N.; Pettit, G. D.; Schmid, H.; Woodall, J. M.; Kern, D. P. *Appl. Phys. Lett.* **1986**, *49*, 1741.
(5) Chiba, D.; Yamanouchi, M.; Matsukura, F.; Ohno, H. *Science* **2003**, *301*, 943.
(6) Ohno, H.; Munekata, H.; Penney, T.; von Molnar, S.; Chang, L. L. *Phys. Rev. Lett.* **1992**, *68*, 2664.
(7) Ohno, H.; Chiba, D.; Matsukura, F.; Omiya, T.; Abe, E.; Dietl, T.; Ohno, Y.; Ohtani, K. *Nature* **2000**, *408*, 944.
(8) Fukuda, Y.; Suzuki, Y.; Sanada, N.; Shimomura, M.; Masuda, S. *Phys. Rev. B* **1997**, *56*, 1084.
(9) Bessolov, V. N.; Lebedev, M. V. *Semiconductors* **1998**, *32*, 1141.
(10) Petrovykh, D. Y.; Long, J. P.; Whitman, L. J. *Appl. Phys. Lett.* **2005**, *86*, 242105.
(11) Tanzer, T. A.; Bohn, P. W.; Roshchin, I. V.; Greene, L. H.; Klem, J. F. *Appl. Phys. Lett.* **1999**, *75*, 2794.
(12) Thelandera, C.; Bjork, M. T.; Larsson, M. W.; Hansen, A. E.; Wallenberg L. R.; Samuelson, L. *Solid State Commun.* **2004**, *131*, 573.
(13) Hang, Q.; Wang, F.; Buhro, W. E.; Janes, D. B. *Appl. Phys. Lett.* **2007**, *90*, 062108. The formulas used for the calculation of electron mobility μ_n are as follows, $g_m = \partial I_{ds}/\partial V_{gs} = (\mu_n C_{ox}/L^2)V_{ds}$, $C_{total} = 2\pi\epsilon_0\epsilon_r L/\cosh^{-1}((r + t_{ox})/r)$.
(14) Affentauschegg, C.; Wieder, H. H. *Semicond. Sci. Technol.* **2001**, *16*, 708.
(15) Bryllert, T.; Wernersson, L.-E.; Froberg, L. E.; Samuelson, L. *IEEE Electron. Device Lett.* **2006**, *27*, 323.
(16) Lind, E.; Persson, A. I.; Samuelson, L.; Wernersson, L.-E. *Nano Lett.* **2006**, *6*, 1842.
(17) Bjork, M. Doctoral thesis, Lund University, Sweden, 2004.
(18) http://www.ioffe.rssi.ru/SVA/NSM/Semicond/InAs/basic.html.
(19) Wang, F.; Dong, A.; Sun, J.; Tang, R.; Heng, Y.; Buhro, W. E. *Inorg. Chem.* **2006**, *45*, 7511.
(20) ICDD-PDF file 00-015-0869.
(21) Johansson, J.; Karlsson, L. S.; Patrik, C.; Svensson, T.; Martensson, T.; Wacaser, B. A.; Deppert, K.; Samuelson, L.; Seifert, W. *Nat. Mater.* **2006**, *5*, 574.
(22) Korgel, B. A. *Nat. Mater.* **2006**, *5*, 521.
(23) McGuiness, C. L.; Shaporenko, A.; Mars, C. K.; Uppili, S.; Zharnikov, M.; Allara, D. L. *J. Am. Chem. Soc.* **2006**, *128*, 5231.
(24) Wang, D.; Wang, Q.; Javey, A.; Tu, R.; Dai, H.; Kim, H.; McIntyre, P. C.; Krishnamohan, T.; Saraswat, K. C. *Appl. Phys. Lett.* **2003**, *83*, 2432.
(25) Castner, D. G.; Hinds, K.; Grainger, D. W. *Langmuir* **1996**, *12*, 5083.
(26) Petrovykh, D. Y.; Sullivan, J. M.; Whitman, L. J. *Surf. Interface Anal.* **2005**, *37*, 989.
(27) Tanuma, S.; Powell, C. J.; Penn, D. R. *Surf. Interface Anal.* **1993**, *21*, 165.
(28) Petrovykh, D. Y.; Yang, M. J.; Whitman, L. J. *Surf. Sci.* **2003**, *523*, 231.
(29) Fukuda, Y.; Suzuki, Y.; Sanada, N.; Shimomura, M.; Masuda, S. *Phys. Rev. B* **1997**, *56*, 1084.
(30) Ichikawa, S.; Sanada, N.; Utsumi, N.; Fukuda, Y. *J. Appl. Phys.* **1998**, *84*, 3658.
(31) Suzuki, S.; Harada, S.; Kosugi, R.; Senzaki, J.; Cho, W.; Fukuda, K. *J. Appl. Phys.* **2002**, *92*, 6230.
(32) MEDICI, www.nanohub.org.
(33) Tersoff, J. *Phys. Rev. Lett.* **1984**, *52*, 465.
(34) Spicer, W. E.; Lindau, I.; Skeath, P.; Su, C. Y.; Chye, P. *Phys. Rev. Lett.* **1980**, *44*, 420.
(35) Hasegawa, H.; Ohno, H. *J. Vac. Sci. Technol. B* **1986**, *4*, 1130.
(36) Woodall, J. M. IEEE Nanotechnology Conference, Cincinnati, OH, 2006.

NL071888T